Materials Research. 2022; 25:e20220079
DOI: https://doi.org/10.1590/1980-5373-MR-2022-0079

Thermal Aging Effects on Mechanical and Intergranular Corrosion Resistance of Super-Austenitic Stainless Steel exposed at 600˚C

A.S.M Cardoso[a*], *J.M. Pardal*[a], *A.P. Souza*[a], *S.S.M. Tavares*[a], *C.S.C. Nogueira*[a], *Y. Xing*[a], *J.L. Cardoso*[b], *M.J.G. Silva*[b], *J.A.C. Velasco*[c]

[a]*Universidade Federal Fluminense (UFF), São Domingos, Niterói, RJ, Brasil.*
[b]*Universidade Federal do Ceará (UFC), Benfica, Fortaleza, CE, Brasil.*
[c]*Instituto Nacional de Tecnologia (INT), Saúde, Rio de Janeiro, RJ, Brasil.*

Received: February 17, 2022; Revised: April 24, 2022; Accepted: April 27, 2022

Super-austenitic stainless steels (SASS) are alloys with better performance in industrial applications in comparison with standard degrees of austenitic stainless steels (ASS), mainly because of elevated Ni and Mo contents and residual control of certain elements because the improvement of refine techniques. These facts, promotes an improvement of mechanical properties and minimize detrimental effects of intergranular corrosion. Besides, some industrial applications involve high temperatures services, because these alloys families have an excellent creep and oxidation resistances performances. In this work, the objective is evaluate the microstructural and mechanical properties in high Mo SASS exposed at 600˚C in specimens aged until 2000 hours. Thus, hardness and toughness values and Double Loop Electrochemical Potentiodynamic Reactivation (DL-EPR) measurements were analyzed in several thermal aging in comparison to solution treatment condition. Complementary, analysis by Light Optical (LOM), of specimens tested by DL-EPR, and Scanning Electron Microscopies (SEM) in fractured surface from Charpy specimens were also analysed by SEM by backscattered electron mode (BSE). The results show that the aging provokes intergranular embrittlement by inhomogeneous distribution in grain boundaries of Mo rich phase precipitation.

Keywords: *Super Austenitic Stainless Steels, Thermal Aging, Mechanical Properties, Corrosion Resistance, Double Loop Electrochemical Potentiodynamic Reactivation.*

1. Introduction

Superaustenitic stainless steels (SASS) are high-performance ferrous alloys used in a variety of aggressive means. In this alloy familiy, the AL-6XN PLUS designation have elevated corrosion resistance, because higher Cr, Ni, Mo e N contents. The alloy is specifically applied in the chemical industries in components such as chemical process tanks and pipelines, process systems for offshore oil and gas platforms, condensers, heat exchangers and piping containing seawater or crude oil, filter washers, vats, and press rolls in pulp bleaching plants, Power plant flue gas scrubber environments, Tall oil distillation columns and packing, desalination equipment and pumps, service water piping systems for nuclear power plants, pharmaceutical equipment (for product purity) and food processing equipment[1].

Nevertheless, some SASS are exposed in high temperatures during services, which can promote a further decrease of corrosion resistance and mechanical properties, when correlated with sensitization in crystalline defects, revealed by electrochemical and Charpy tests. Thus, Hao et al.[2] observed the austenitic matrix decomposition in aging temperatures between in 600 ºC for 1 h, that results in the formation of the secondary phase mainly in grain boundaries for SASS with 20.5%Cr-16.2%Ni-7.3%Mo-0.4%N[3].

Koutsoukis et al.[4] report that it is well known that the sigma phase is the most common and important intermetallic phase in superaustenitic stainless steels. The precipitation behavior of this phase varies depending on many factors, such as chemical compositions and thermal aging conditions. In particular, the sigma phase is a hard and brittle phase, being notorious for reducing the toughness of the alloy[5].

Phillips et al state that the most important intermetallic phase formed in SASS 654SMO was the σ phase, which would be the main intermetallic phase responsible for the deterioration in the mechanical properties SASS. This is due to the fact that the triple-point junction is preferably Cr and Mo concentration sites, resulting in increased precipitation kinetics of the secondary phases. It also states that in temperatures ranging from 700 to 1100 ºC, carbides are usually the first to form and in longer aging times, these carbides are usually replaced by intermetallic compounds such as σ phase, in addition to the slow diffusion of the substitutable elements in austenite, the σ phase being incoherent with austenite, thus making it difficult to nucleate[6,7].

Meng et al report on his research on precipitation behavior in the SASS AL-6XN®, which is the predecessor alloy of the AL-6XN PLUS™, which in thermal aging at 600 °C for 1200 hours, some discontinuous precipitates of phase σ with cuboid-like morphology were easily observed

*e-mail: *bra_afs@hotmail.com*

at the grain limits. The chemical composition of phase σ precipitated in SASS AL6XN at 650°C is about 21.2% Cr, 37.8% Fe, 14.7% Ni, 20.4% Mo, and 5.9% Si. The nucleation mechanism was proposed to be associated with the dissolution of $M_{23}C_6$ carbides in grain boundaries in most SASS, due to high interfacial energy of the precipitated interface/austenite[8].

The precipitation of intermetallic compounds generates the phenomenon of sensitization in SASS, being one of the most harmful types of corrosion, intergranular corrosion. Sensitization may originate from heat treatments, welding, slow cooling, through the temperature range of sensitization or working conditions in this range[9].

As a result, we seek the metallurgical knowledge of this material, which will allow to determine reliable guidelines on the thermomechanical processing of the alloy, in order to increase the service life of equipment and pipes, as a consequence increasing the time interval between maintenance and/or replacement. This work aims to investigate the sigma phase precipitation in the SASS 22Cr-25Ni-7Mo alloy and its effect on mechanical properties and corrosion resistance resulting from thermal aging up to 2000 h.

2. Experimental

Samples with 10 mm x 10 mm x 3.7 mm and subsize Charpy specimens with 55 mm x 10 mm x 5mm were obtained by machining from a SASS AL-6XN PLUS plate with chemical composition showed in Table 1. The solution treatment and several aging conditions were performed in triplicate in the values showed in Table 2.

For aging treatments, a computational thermodynamic simulation was previously performed to identify the temperature range of sensitization of the studied alloy, using the Thermocalc®. The thermal aging of 600 ºC was chosen mainly because several industrial components working near this temperature, but also was considered the kinetics of several precipitation phases in this temperature, such as is evaluated in a conventional austenitic stainless steel (ASS).

Charpy test was conducted in a universal pendulum with 0-300J +/-1J at 25 ºC for determinate the Toughness in all conditions. Additionally, the lateral expansion from each specimen was also determinate. After this, the surface fracture was preserved in several conditions to perform an analysis by stereo microscope and SEM for evaluates changes in a mechanism of fracture behavior.

The samples were also evaluated by Light Optical Microscopy (LOM) and Scanning Electron Microscopy (SEM), where the etchings showed in Table 3 were applied for purpose to evaluates and distinguish several and important microstructural aspects during aging treatments.

Several hardness test were employed to evaluate the behavior of SASS studied by aging, where laboratorial and portable field equipment´s were employed. In conventional test were performed 8 (eight) measurements by HRB and Vickers scales taking into account ASTM E18-14[11] recommendations. Thus, complementary hardness measurements were performed with of Portable Ultrasonic Contact Impedance (UCI) for potential field application.

Double Loop Electrochemical Potentiodynamic Reactivation (DL-EPR) test were performed, in triplicate for all studied conditions, using a portable cell as described[12]. The test solution was composed of 0.5 M H_2SO_4 + 0.5 M NaCl[10]. All tests were conducted with a scan rate of +/-1m V/Sec after stabilization of open circuit potential (OCP) value until 0.3 V(SCE) and after this was reverse the scan at OCP value again. The Degree of Sensitization (DOS) were obtained, for each sample studied, by reactivation (Ir) and activation (Ia) current peaks values ratio. Figure 1 showed an example of result of DL-EPR test applied by portable mode [Brigida] with potential field nondestructive application.

The DL-EPR and volume fraction of deleterious phase (DPPF) results, obtained by metallographic replica studied like B.B. Almeida et al.[13]. The electrical resistivity test was performed as described by Girotto and Santos[14] using the 4-pointed or 4-terminal method. The measurements were performed using a DC source and two multimeters of 61/2 digits of precision, where the current was injected into the surface of each sanded sample to 400 particle size sandpaper. However, the geometric dimensions of each sample were obtained with the aid of a digital calibrated to estimate the geometric correction factors to be applied later in the statistical treatment of the obtained data.

3. Results and Discussion

3.1. Computational thermodynamics simulation

The result of the computational thermodynamic simulation for the chemical composition of the AL-6XN PLUS alloy, revealed the temperature of 1150 ºC as suitable for the treatment by thermal solution, as can be seen in Figure 2,

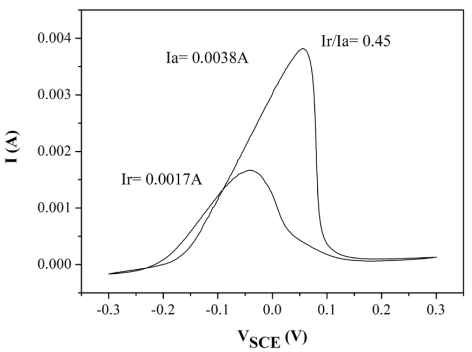

Figure 1. DL-EPR test performed at room temperature for the condition of 500 h of aging time.

Table 1. Chemical composition by optical emission spectroscopy (% by weight) of SASS AL-6XN PLUS[10].

Designation UNS	Trade Name	Weight (% Fe balance).						
		C	N	Mn	Si	Cr	Ni	Mo
N08367	AL-6XN PLUS	0.02	0.24	0.35	0.32	21.80	25.80	7.60

in which the matrix is completely austenitized, although the manufacturer uses lower solution treatment temperatures of around 1110 ºC to dissolve any possible precipitate that may form during the manufacturing process[1]. It is also noteworthy that the simulation was performed in a range of 500 to 1200 ºC evaluating the phases in equilibrium and their chemical composition every 50 ºC. Still in Figure 2 stand out the intermetallic phases in equilibrium highlighting the aging analysis temperature with a vertical dashed line at 600 ºC. It is possible to observe that between 500 and 730 ºC, there is a small increase in the percentage of austenite. Similarly, the percentage of deleterious phases in equilibrium presents the highest percentages for the same temperature range, especially the sigma phase.

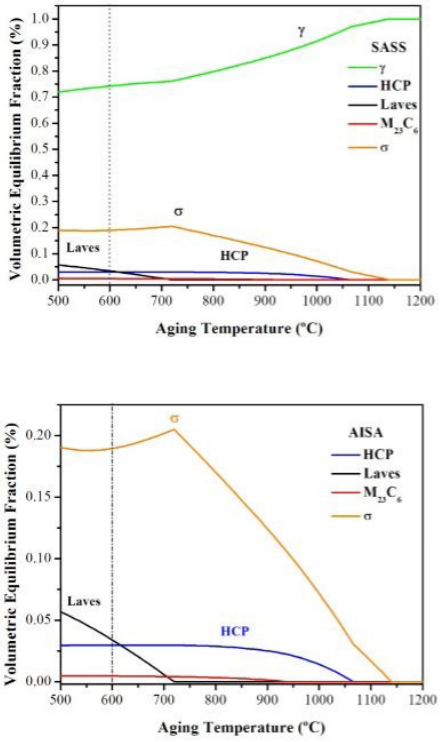

Figure 2. AL-6XN PLUS equilibrium precipitated phases obtained with Thermocalc® for the temperature range from 500 to 1200 ºC.

Table 2. Solution treatment condition and several aging conditions adopted for this work.

Solution treatment	Thermal aging at 600 ºC
1150 ºC for 30 min.	0 h (Not Aged)
	250 h
	500 h
	750 h
	1000 h
	1500 h
	2000 h

Table 4 shows the chemical composition in equilibrium of the possible phases present using Thermocalc® highlighting that intermetallic compounds exhibit high molybdenum and chromium contents and with crystallography hexagonal compact (HCP). This simulation is fundamental for the identification of the types of precipitates present in the grain boundaries of the conditions studied by SEM analysis using energy dispersion spectroscopy (EDS)

3.2. Mechanical properties

Figure 3 shows the behavior of Rockwell B (HRB) and Vickers (HV) hardness for the various study conditions from 0 h of thermal aging (solution treatment only). In the HRB curve, a slight increase in hardness under aging conditions of up to 1000 h stands out, although larger aging's provide a possible fall in the values of this property. In the 1500 and 2000 h conditions, a great dispersion is seen in the values. In the HV curve, there is an increase of this property for 500 h of thermal aging, presenting a similar behavior to the values presented in the Rockwell B hardness test, where a small increase occurs in the interval between 250 and 750 h of thermal aging compared to the solution treatment condition. In the Vickers hardness curve, increasing values are observed in the period from 250 to 500 h, and it is not possible to ensure a change in the behavior of this property for the thermal aging condition of 750 h due to the high dispersion of the results. In the aging above 1000 h, close values are observed in relation to the solution treatment condition.

On this condition, Pelliccione et al.[15] and Perdomo and Spry[16] mentioned that phase precipitation σ does not significantly increase hardness values with low percentage values[17].

The measures of impact toughness and percentage lateral expansion present similar behavior and reveal a fragility of the material during the aging time, as can be observed in the curves of Figure 4, respectively. In the following images, it is possible to identify a total fragility in aging conditions

Table 3. Etching employed to LOM and SEM analysis.

Characterization Technique	Etching	Composition	Etching Methodology	Purpose
LOM	Oxalic acid	10% aqueous solution	Electrolytic 3V for 50 sec with sample in positive electrode (anode)	Reveal the microstructure of the samples as received and solution treatment
	KOH	20% aqueous solution		Reveal the sigma phase of aged samples
SEM	Regal water	(1:3) + 50% H_2O	Direct application for 3 min.	Reveal the microstructure and intermetallic precipitates of aged samples

above 750 h where the precipitation of intermetallic phases is manifested in a heterogeneous way. Additionally, it is observed that the dispersion of the toughness values is also affected by morphological and compositional changes of the intergranular precipitates.

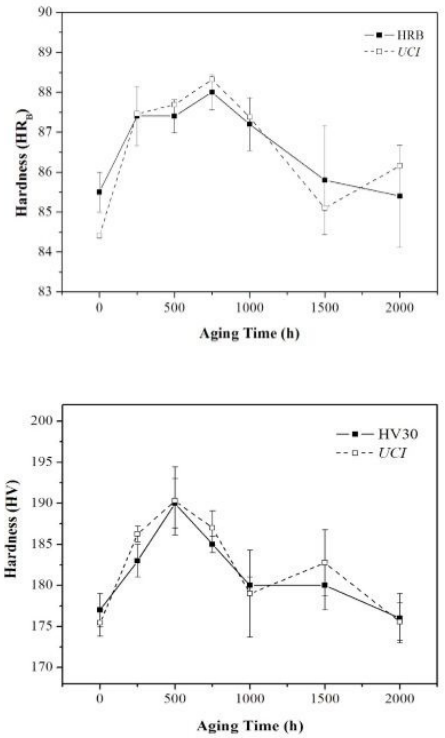

Figure 3. Comparison between Rockwell B and Vickers laboratory and field hardness values of solution treatment and isothermally aged samples at 600 ºC.

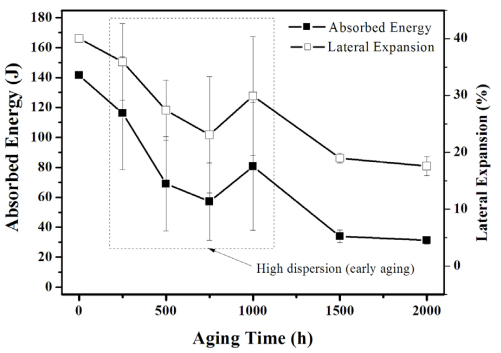

Figure 4. Values of toughness and lateral expansion of the material studied under several aging conditions at 600 ºC.

Although they were evaluated in duplicate in the test specimens (PC) tested, a high dispersion in the values obtained was considered, mainly in the 1000 h aging condition, which motivated the realization of two complementary tests for the conditions of 250 to 1000 h, to achieve more robust results. This phenomenon is mainly attributed to the high heterogeneity in precipitation sites and morphological changes resulting from intermetallic precipitation in the austenite grain boundaries presented in item 3.4.

In Figure 5a and b it is possible to analyze the fracture surfaces of the solution treatment (ST) and aged (A) conditions for 250 h. As expected, the solution treatment condition exhibits a large lateral expansion with a relevant shear region externally framing the fracture surface of the test body, in addition, clear signs of plastic deformation, typical of this type of fracture, which resulted in an absorbed energy of 141.5 J. Already at 250 h of aging, attention is made for a fracture mechanism similar to the previous case, although the shear region prevails with a smaller area when compared to the solution treatment condition. However, the matte aspect and clear signs of deformation resulted in an absorbed energy of 112J. In Figure 4c and d of the thermal aging condition for 500 h, a drastic reduction of the shear region is observed that frames the surface of the test body, in addition, signs of fracture with a bright aspect are divided in addition to a lateral expansion that is not significant in relation to the previously described cases. These facts resulted in an absorbed energy of 56J. The thermal aging condition of 750 h shows a smaller lateral expansion, highlighting a radial zone with rapid propagation of the crack from the notch, also displaying signs of a shiny-looking surface, as can be seen in Figure 5d. Figure 5e and f presents the fracture surface of two specimens aged for 1000 h, which highlights a paradoxical behavior resulting from heterogeneity, as well as variations in chemical and morphological composition of precipitates resulting in the condition of Figure 5e with fibrous aspect and evidence of plastic deformation, while Figure 5f denotes a fragile aspect with an important radial zone. Finally, the fracture surface of the 1500 h and 2000 h CPs are presented in Figure 5g and h. In these cases, a completely fragile fracture presenting a characteristic bright aspect of fragility, although a small lateral expansion is observed. Comparing with the other fractures, both samples presented the lowest values of lateral expansion, in addition to the lowest values of absorbed energy, to the detriment of the longer times of thermal aging.

Table 4. Possible chemical composition (% weight) of the equilibrium phases in AL-6XN PLUS at 600 ºC, obtained with Thermocalc®.

Phases	Fe	Ni	Cr	Mo	Si	N	C
FCC	51.88	32.67	13.22	1.77	0.46	0.00	0.00
HCP	0.03	0.05	71.22	18.01	0.00	10.63	0.05
$M_{23}C_6$	5.14	0.56	68.48	20.02	00.00	00.00	5.84
Laves	0.00	0.00	0.46	49.70	0.04	0.00	0.00
Sigma	28.80	10.72	39.01	21.47	0.00	0.00	0.00

Figure 5. Fracture surface of Charpy specimen´s performed: (a) ST (b) 250 h, (c) 500 h, (d) 750 h, (e and f) 1000 h, (g) 1500 h and (h) 2000 h.

3.3. Double Loop Electrochemical Potentiodynamic Reactivation (DL-EPR)

The DL-EPR assays were performed in triplicate for all proposed aging conditions and in the solution treatment sample. Only the samples of 500h, 1000h, 1500h and 2000h of thermal aging showed curves with reactivation peaks (Ir). Under the condition of aged for 500 h, a significant reactivation peak was detected, resulting in an Ir/Ia= 0.45.

This fact reinforces that compositional and morphological aspects of precipitates, as well as their distribution, play a significant role in the characterization by this technique, keeping a certain similarity with the results obtained by the hardness assay in this interval. A behavior with large reactivation peaks was obtained in samples aged for 1500 h and 2000 h, with Ir/Ia= 0.47 and 0.77, respectively. In these conditions, signs of microstructural degradation are evidenced as a consequence of the intense precipitation of intermetallic compounds along the grain boundaries of austenite.

Figure 6 describes how the sensitization values obtained by the DL-EPR results vary according to the aging time at 600 ºC for SASS AL-6XN PLUS in tests at room temperature. There is a first sensitization peak at 500 h with a strong dispersion in the results as a consequence of compositional and/or morphological changes combined with heterogeneous intergranular precipitation. However, this dispersion is still observed in aging at 1500 and 2000 h, however there is a high degree of sensitization in these conditions, if compared to those previously described. Although they were performed in triplicate for each treatment condition, there is a strong dispersion in the results as a consequence of compositional and/or morphological changes combined with heterogeneous intergranular precipitation. However, this dispersion is still observed in aging at 1500 and 2000 h, however there is a high degree of sensitization in these conditions, if compared to those previously described.

The DL-EPR assays were performed in triplicate for all proposed aging conditions and in the solution treatment sample. Only the samples of 500 h, 1000 h, 1500 h and 2000 h of thermal aging showed curves with reactivation peaks (Ir) and the other conditions showed no reactivation peak (Ir= 0). In the condition of aging for 500h, significant reactivation peaks with low dispersion were detected, resulting in the average value of Ir/Ia= 0.45.

3.4. Microstructural characterization

The samples solution treatment and aged up to 2000 h after etched were analyzed by SEM through images obtained by secondary electrons (SE) and backscattered (BSE) using complementary energy dispersive spectroscopy (EDS). In the solution treatment sample, the presence of precipitates or relevant tertiary phases was not detected, being in accordance with the ATI METALS manufacturer's compliance criteria[18]. In the sample aged thermally for 500 hours it is possible to identify coarse precipitates mainly in the triple points of the grains, as observed in Figure 7. The chemical composition of the precipitate identified as sigma phase (σ) and of the austenitic microstructure (γ) are shown in Table 5, where high values of Fe, Ni, Cr and Mo, as expected due to the varied stoichiometry in the SASS as $(FeNi)_x(CrMo)_y$.

In the sample aged thermally for 500 hours it is possible to identify coarse precipitates of the sigma phase, mainly in the triple points of the grains, as observed in Figure 7. The chemical composition is shown in Table 5, where high

Table 5. Chemical composition (% weight) of precipitate analyzed by SEM EDS.

Phase Element	Percentage of the element		
	Spectrum 6	Spectrum 7	Spectrum 8
	σ	γ	γ
Fe	36.9	44.9	45.1
Cr	28.5	22.6	22.7
Ni	12.9	25.3	24.7
Mo	21.3	7.0	7.2
Si	0.4	0.3	0.3

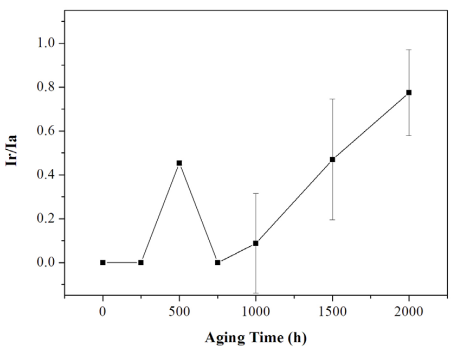

Figure 6. Degree of sensitization (Ir / Ia) of AL-6XN PLUS samples versus aging time at 600ºC.

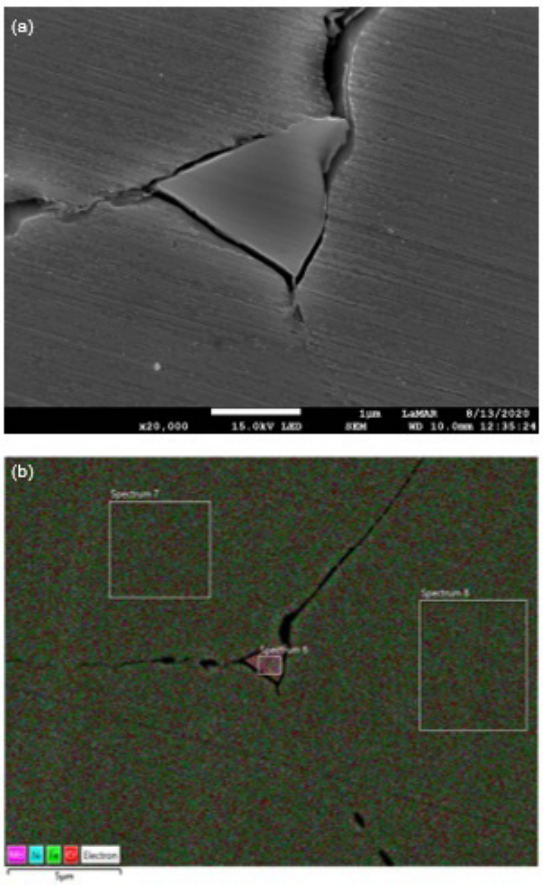

Figure 7. Discontinuous intergranular precipitates aging for 500 h. Image obtained in SEM with (a) 20000X in secondary electron (SE) mode and (b) Precipitate with Mo rich region.

values of Fe, Ni, Cr and Mo, as expected due to the varied stoichiometry in the SASS as $(FeNi)_x(CrMo)_y$.

The coarse precipitates have a certain globular appearance; however, there is also a discontinuous lamellar precipitation along the grain boundaries. The precipitation of these compounds has a direct relationship with the low toughness values presented as a consequence of the intergranular embrittlement process.

Figure 8 presents the condition of 1500 h of thermal aging where more intense precipitation is observed in the grain contours. Precipitates present predominantly fine lamellar morphology and in some regions a tendency to small globular morphology arranged discontinuously along the grain contours and also observed in the triple points as in the sample of 500 h. Intergranular precipitation under this condition drastically affected the toughness values, with the lowest values in relation to previous aging conditions.

Figure 9 shows the condition of 2000 h of thermal aging, it was possible to identify clusters of intense coarse precipitation. It is worth noting a heterogeneous precipitation similar to that, which occurred in samples aged for 1500 h, having reached values close to toughness.

It is interesting to note that studies conducted on alloys with a chemical composition close to the AISA AL-6XN$^+$ obtained results quite adherent to those mentioned here. In this context, Song et al [19], carried out isothermal treatments for 1 h in the interval between 650-1100ºC in the 654SMO alloy, identifying the sigma phase as preponderant, among others, such as, Cr_2N, phase μ, phase χ, Laves phase, $M_{23}C_6$, M_6C e M_3C. According to Y. Hao et al[2], the behavior of a SASS 20Cr-24Ni-6Mo alloy in thermal aging, where observations similar to the present study were verified by SEM and transmission electron microscopy (TEM) in aging in the range between 625 and 1050 ºC, in which the sigma phase was detected mainly, although it is also noted that the Laves phase was detected only in the range of 625 to 825 ºC.

3.5. Electrical Resistivity DC

Figure 10 shows the average values of electrical resistivity performed at room temperature. As observed for aging at 600 ºC, there is a sharp drop in resistivity from 0 h to 750 h,

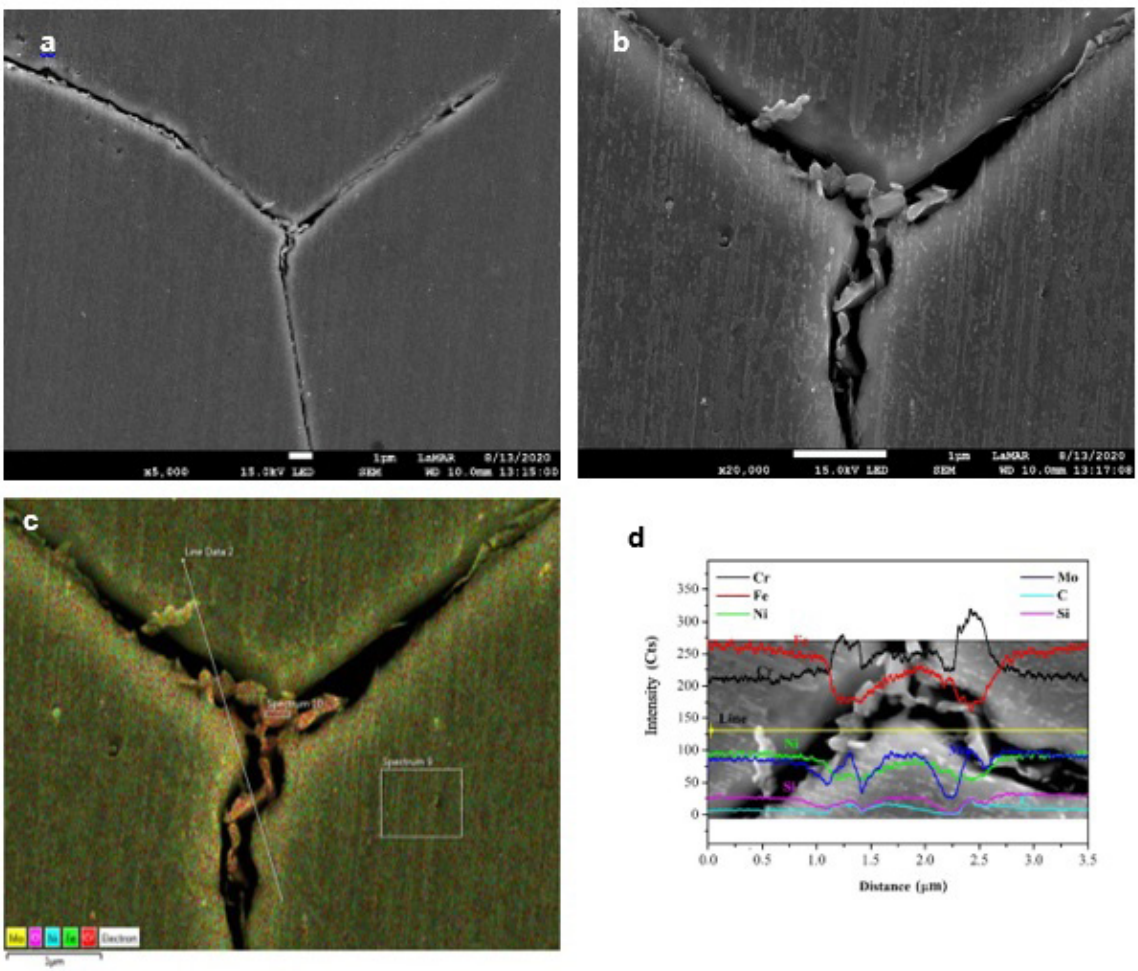

Figure 8. Discontinuous intergranular precipitates in thermal aging for 1500 h. Image obtained in SEM with (a) 5000X and (b) 20000X in secondary electron (SE) mode, (c) EDS map denoting the regions rich in Mo and (d) line scan denoting the regions rich in Fe, C, Cr, Ni, Mo and Si.

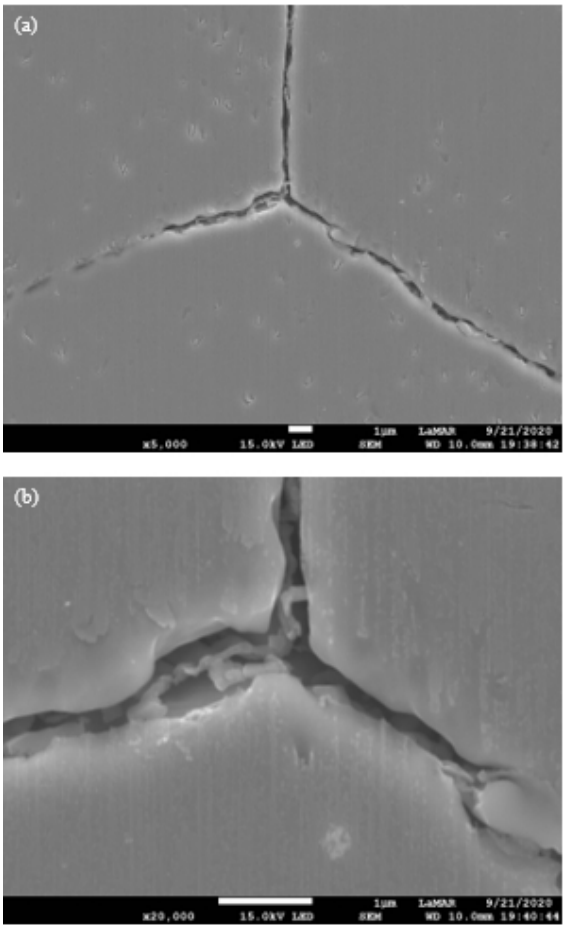

Figure 9. Discontinuous intergranular precipitates aging for 2000 h. Image obtained in SEM with (a) 5000X and (b) 20000X in secondary electron (SE) mode.

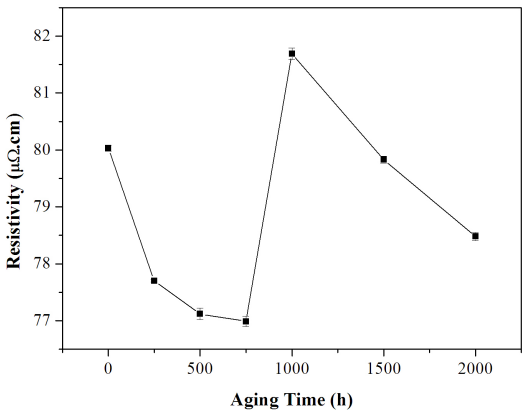

Figure 10. DC resistivity of studied samples.

where the microstructures present coarse precipitates rich in Fe, Ni, Cr and Mo. At 1000 h of aging, there is a marked increase in this property, which is linked to the morphological change of the precipitates, which are fine (lamellar) at the grain boundaries and at the triple points on the limits of the austenitic microstructure.

The drop between the values from 1000 h to 2000 h appears again, however, with values higher than the values reached from 0 h to 750 h, due to the morphological changes of the lamellar precipitates increasingly thin and dispersed along the grain boundaries.

The measurements show sudden changes in resistivity due to compositional and/or morphological changes combined with heterogeneous intergranular precipitation. The presence of intermetallic compounds causes a decrease in this physical property in metal alloys[14,20].

4. Conclusions

Using the database TCFE6 Thermocalc®, it was possible to determine the temperature of 600 °C as more susceptible to the formation of deleterious phases, the primary sigma phase in the greater proportion.

A stage with a possible increase the effect of sigma phase precipitation in hardness between 500 and 750h is highlighted, being linked to the resulting values in the dispersion measurements obtained.

The effects of aging at a temperature of 600 ºC showed good sensitivity in relation to the tests of toughness, manifesting a great change of this property according to the aging time as a consequence of the phenomenon of intergranular fragility affected by sigma phase precipitation with lamellar, globular morphology and discontinues in the contours of the austenitic matrix, evidenced by the results obtained by SEM.

PERC and DL-EPR tests revealed the sensitization in material, with the exception of the aging condition of 600 ºC for 750 h, with a possible redistribution effect of alloy elements and/or changes in existing precipitates, as observed microstructurally in the SEM between 500 h and 1000 h which results in a healing or healing process under this particular aging condition.

The results obtained by the continuous current electrical resistivity (DC) assay showed to be promising, where the resistivity of the austenitic phase showed a great sensitivity in relation to this property, because of the variation of concentration of elements in solid solution, especially in relation to Cr and Mo near the grain contours. This technique can be a valuable tool for detecting microstructural changes resulting from the sensitization process as well as toughness.

The deleterious effect of thermal aging on the mechanical properties and corrosion resistance of SASS AL-6XN PLUS are linked to the precipitation of the sigma phase in the grain boundaries, mainly in the triple points. The results were expected due to heterogeneous precipitation rich in molybdenum in the austenite grain boundaries, this heterogeneity occurs both in the morphology and in the distribution of these precipitates along the boundary. The heterogeneity of precipitation caused a high dispersion of the values obtained in the tests, even carrying out additional tests to corroborate the results.

5. Acknowledgments

Authors acknowledge the brazilian research agencies CAPES, CNPq, and FAPERJ for the financial support.

6. References

1. ATI: Allegheny Technologies Incorporated. Data sheet al-6XN alloy. Springfield: ATI; 2010.
2. Hao Y, Cao G, Li C, Li J, Liu W, Zhang W, Liu Z. The aging precipitation behavior of 20Cr-24Ni-6Mo super-austenitic stainless steel processed by conventional casting and twin-roll strip casting. Mater Charact. 2019;147:21-30.
3. Anburaj J, Nazirudeen SSM, Thillairajan K, Chandrasekar A, Narayanan R. Quantitative analysis of intermetallic precipitates in high mo superaustenitic stainless steel. Appl Mech Mater. 2014;592-594:711-5.
4. Koutsoukis T, Redjaïmia A, Fourlaris G. Phase transformations and mechanical properties in heat treated superaustenitic stainless steels. Mater Sci Eng A. 2013;561:477-85.
5. Fonda RW, Lauridsen EM, Ludwig W, Tafforeau P, Spanos G. Two-dimensional and three-dimensional analyses of sigma precipitates and porosity in a superaustenitic stainless steel. Metall Mater Trans A. 2007;38:2721-6.
6. Phillips NSL, Chumbley LS, Gleeson B. Phase transformations in cast superaustenitic stainless steels. J Mater Eng Perform. 2009;18:1285-93.
7. Tehovnik F, Burja J, Arh B, Vode F. Precipitation of σ phase in superaustenitic stainless steel UHB 904L. Metalurgija. 2017;56(1-2):63-6.
8. Meng L, Xing H, Sun J. Precipitation behavior in AL6XN austenitic stainless steel. Mater Sci Forum. 2010;654-656:2330-3.
9. Magri M, Alonso-Falleiros N. Métodos eletroquímicos para a avaliação da sensitização em aços inoxidáveis martensíticos. In Congr. Anu. Associação Brasileira de Metalurgia, Materiais e Mineração - ABM; 1996; São Paulo. Anais. São Paulo: ABM 1996.
10. Cardoso JL. Avaliação e comparação da resistência à corrosão por pites do aço super austenítico AL 6XN PLUS ™ e dos aços inoxidáveis austeníticos da série AISI 304L, 316L e 317L [dissertação]. Fortaleza: Universidade Federal do Ceará; 2011.
11. ASTM: American Society for Testing and Materials. E18 − 14: Standard Test Methods for Rockwell Hardness of Metallic Materials. West Conshohocken: ASTM; 2014.
12. Alvarez TR. Nondestructive microstructural characterization of superduplex stainless steel by double loop electrochemical polarization reactivation portable test. Mater Res. 2017;20(2):440-6.
13. Almeida BB, Cardoso ASM, Garcia PSP, Igreja HR, Chales R, Noris LF, et al. Nondestructive microstructural characterization of austenitic-ferritic stainless steel welded joints by double loop electrochemical polarization reactivation portable test. Mater Res. 2022;25:e20210283. http://dx.doi.org/10.1590/1980-5373-MR-2021-0283.
14. Girotto EM, Santos IA. Medidas de resistividade elétrica DC em sólidos: como efetuá-las corretamente. Quim Nova. 2002;25(4):639-47.
15. Pelliccione AS, Moraes MF, Galvão JLR, Mello LA, Silva ES. Análise de falhas em equipamentos de processo - mecanismos de danos e casos práticos. Rio de Janeiro: Editora Interciência; 2012.
16. Perdomo JJ, Spry TJ. Sigma Phase Formation of Type 310 stainless steel in a lime kiln burner nozzle. Mater Perform. 2007;46(3):54-7.
17. Ennes CSB. Caracterização microestrutural não destrutiva da degradação de um espelho de gerador de gás inerte construído em AISI 310S. Rio de Janeiro: UFF; 2013.
18. ATI: Allegheny Technologies Incorporated. Data sheet Al-6XN Plus. Pittsburgh, USA: ATI; 2015.
19. Song SG, Pu EX. Precipitated phases of superaustenitic stainless steel 654SMO. J Iron Steel Res Int. 2017;24:743-9.
20. Mori Y, Hashimoto M, Liao J. Effect of surface composition on contact resistivity and corrosion resistance of 316L stainless steel. ISIJ Int. 2013;53(6):1057-61.